SCIENTIFIC REP**O**RTS

OPEN

GLAG theory for superconducting property variations with A15 composition in Nb$_3$Sn wires

Yingxu Li[1,2,3] & Yuanwen Gao[1,2]

We present a model for the variation of the upper critical field H_{c2} with Sn content in A15-type Nb-Sn wires, within the Ginzburg-Landau-Abrikosov-Gor'kov (GLAG) theory frame. H_{c2} at the vicinity of the critical temperature T_c is related quantitatively to the electrical resistivity ρ, specific heat capacity coefficient γ and T_c. H_{c2} versus tin content is theoretically formulated within the GLAG theory, and generally reproduces the experiment results. As Sn content gradually approaches the stoichiometry, A15-type Nb-Sn undergoes a transition from the dirty limit to clean limit, split by the phase transformation boundary. The H-T phase boundary and pinning force show different behaviors in the cubic and tetragonal phase. We dipict the dependence of the composition gradient on the superconducting properties variation in the A15 layer, as well as the curved tail at vicinity of H_{c2} in the Kramer plot of the Nb$_3$Sn wire. This helps understanding of the inhomogeneous-composition inducing discrepancy between the results by the state-of-art scaling laws and experiments.

At present, conventional low-temperature superconductors such as Nb$_3$Sn have been extensively applied in high-energy and nuclear physics, as well as in magnetic resonance imaging systems[1]. Inhomogeneity of Sn content is inevitable in practical Nb$_3$Sn conductors, due to the high vapor pressure of Sn at the formation temperature of the A15 phase in a solid-state diffusion reaction[2, 3]. The tin variation in a conductor covers nearly the entire A15 phase field of binary Nb$_{1-\beta}$Sn$_\beta$ with $\beta = 0.18 \sim 0.255$[4]. In a Nb$_3$Sn conductor, the Sn gradient across the A15 layer has a remarkable impact on the local variation of the superconducting properties[5]. Experiments show that, the upper critical field B_{c2} varies almost linearly at ~5 T per at% between 19.5% and ~24 at% Sn, and the transition temperature T_c versus tin concentration β also exhibits a linear relation within nearly the entire A15 phase field[3]. When β approaching stoichiometry of Nb$_{1-\beta}$Sn$_\beta$, $\beta \approx 24$ at%, T_c (or B_{c2}) versus β no longer keeps the linear relationship due to the lattice softening (decreasing in phonon frequency)[6], which means the varying Sn content leads to the cubic-tetragonal phase transformation of A15 lattices. The alloying addition (Ti and/or Ta), which is introduced in most modern high-field Nb$_3$Sn conductors for increasing the electrical resistivity, suppressing the martensitic phase transformation and thus raising B_{c2}, also becomes approximately linear with the Sn content β[7]. As for other additives, the ZrO$_2$ precipitates in Nb$_3$Sn wires could refine Nb$_3$Sn grain size such that change the pinning behavior[8].

For Nb$_3$Sn wires, the scaling law and the experiment show a disagreement in the field dependence of the pinning force at high reduced fields[9]. One of the reasons could be the inhomogeneity of microstructure and composition[9]. This also explains the observation that the scaling field lies below the experimental B_{c2} of Nb$_3$Sn wires. In fact, the scaling field for the critical current reflects the average properties over the wire volume; it thus relates to the local variation of the critical field dependent on the composition gradient[10]. Cooley and the coauthors simulate the effect of Sn composition gradients on the superconducting properties of powder-in-tube (PIT) Nb$_3$Sn strand, with an ideal structure modeled by concentric shells with varying Sn content[7]. They found that different Sn profiles have a pronounced effect on the irreversibility fields defined by the extrapolation of Kramer plots H_K, and also that Sn gradients reduce the elementary pinning force, H_K and the critical current density J_c[7].

The temperature dependence of the upper critical field $H_{c2}(T)$ in inhomogeneous Nb$_3$Sn conductors, as the field-temperature phase boundary, is comprehensively investigated by Godeke et al.[2]. It is concluded that, the

[1]Key Laboratory of Mechanics on Environment and Disaster in Western China, Lanzhou University, The Ministry of Education of China, Lanzhou, Gansu, 730000, P.R. China. [2]Department of Mechanics and Engineering Science, College of Civil Engineering and Mechanics, Lanzhou University, Lanzhou, Gansu, 730000, P.R. China. [3]Department of Engineering Mechanics, School of Mechanics and Engineering, Southwest Jiaotong University, Chengdu, Sichuan, 610031, P.R. China. Correspondence and requests for materials should be addressed to Y.G. (email: ywgao@lzu.edu.cn)

complete field-temperature phase boundary can be described with the simplest form of the Maki-DeGennes (MDG) relation, and independent of compositional variation, measuring technique, criterion for the critical field and strain state[2].

Various experiments[11–13] and models[14, 15] have recently been conducted to investigate the dependence of the superconductivity and magnetic properties of Nb_3Sn samples on Sn content and disorder. The underlying physics for the superconducting properties variation with the A15 composition in Nb_3Sn is however still not very clear. The already-existing physical formulas for this dependence are insufficient for describing the state-of-art experimental results of binary Nb_3Sn samples and practical Nb_3Sn wires. In this paper, we develop a series of formulas based on GLAG theory; with respect to the previous formulas, the present ones systematically describe the major behaviors of the relevant experimental phenomena: the composition dependence of H_{c2}, phase boundary and pinning behaviors. By this way, new physical insights into the importance of the composition inhomogeneity are provided. As for practical engineering significance, tin composition and possible additives are important for the very high J_c now achieved in commercial strands[16, 17]. Therefore, describing the superconducting properties dependence on the A15 composition in theory will facilitate the understanding of the optimization for the critical current density J_c. Based on the above considerations, it is of importance to investigate the physical mechanism of the superconducting properties dependences in inhomogeneous Nb_3Sn samples.

In this paper, We model the variation of the upper critical field H_{c2} with Sn content in A15-type $Nb_{1-\beta}Sn_\beta$, within the GLAG theory frame. In this theory, the occurrence of H_{c2} is due to the breaking of orbital pair and the Pauli paramagnetic limiting. Two scattering mechanisms should be considered in type-II superconductors like Nb_3Sn: electron-transport scattering by impurity (disorder) and spin-orbit scattering. As for A15 Nb_3Sn, composition inhomogeneity and its deviation from stoichiometry may cause defect and site disorder in Nb_3Sn lattices[4], which contribute most to the scattering by impurity. Based on this physical picture, H_{c2} is correlated to the superconductivity parameters (the coherence length, the London penetration depth and etc.) as well as the scattering characteristics (the mean free path of electron transporting). As for the strong-coupling superconductor like Nb_3Sn, one should include the correction for electron-phonon interaction to the weak-coupling BCS value. Since the microscopic parameters mentioned above cannot be determined directly, we correlate them to the transition temperature, normal-state resistivity and coefficient of electronic heat capacity. The three material parameters have been extensively measured as a function of tin content[3, 4, 18, 19]. In this manner, we can determine the superconducting properties variation with composition concentration. The following section will present the detail.

Model

Upper critical field at vicinity of superconducting transition temperature.
The best quality Nb_3Sn samples, with highest transition temperature T_c's and resistance ratios ($RRR = \rho(300\,K)/\rho(20\,K)$), have very narrow resistive transitions[19]. The transitions tend to broaden in high fields. Measured ternary PIT wire also exhibits a narrow transition at a wide range of fields and temperatures[2]. At the vicinity of T_c, the upper critical fields $H_{c2}(T)$ are thus nearly the same, and almost independent on the selected critical-state criterion. We are then allowed to determine H_{c2} near T_c uniquely. The resistivities ρ near T_c are approximated as $\rho(T_c)$, measured at temperatures just above T_c, and the coefficient of electronic heat capacity γ remains a constant at the vicinity of T_c, satisfying the low-temperature heat capacity formula without undergoing a specific heat jump.

In the microscopic physical concept, the scattering of impurity (Supplementary Information A and Fig. A1) enters into the superconductivity of type II superconductors by changing the Ginzburg-Landau (GL) parameter κ at the vicinity of T_c. We have κ in two limiting cases, $\kappa_{clean}(T) = \kappa(T_c)\chi_1(T)$ without scattering effect and $\kappa_{dirty}(T) = \kappa_{dirty}(T_c)\chi_2(T)$ relevant to scattering, where $\kappa_{clean}(T_c) \approx 0.96\delta_L(0)/\xi_0$ and $\kappa_{dirty}(T_c) = 0.72\delta_L(0)/l$ (see Supplementary Information B for GLAG description of the superconductivity parameters). Here, $\delta_L(0)$ is the London penetration depth of the magnetic field at 0 K. ξ_0 is the standard coherence length. l is the mean free path of electron transporting. κ_{clean} and κ_{dirty} refer to the clean limit ($\xi_0 \ll l$) and dirty limit ($\xi_0 \gg l$), respectively. $\chi_1(T)$ and $\chi_2(T)$ represent the temperature dependence of κ for the clean limit and dirty limit, respectively; calculations show that they vary little with T near T_c, $\chi_1(T) \approx \chi_2(T) \approx 1$[20].

In light of the classic proposal[19, 21], the superconductivity parameters $\delta_L(0)$, ξ_0 and the scattering parameter l involved in the GL parameter κ can be linked to three independent material parameters, the transport scattering resistivity ρ, the low-temperature coefficient of electronic heat capacity γ and the superconducting transition temperature T_c. Assuming a spherical Fermi surface and isotropic metal, we are allowed to use the electron conduction formula Eq. (A1) and the electron heat capacity relation Eq. (C1) in the GLAG description of the superconductivity parameters (Supplementary Information C), and then express l, ξ_0, $\delta_L(0)$, κ_{clean} and κ_{dirty} as functions of ρ, γ and T_c, Eqs. (C15)–(A19). Including the correction for the anisotropy in Nb_3Sn (Supplementary Information D), one must consider the change of Fermi surface shape from the isotropic model, which leads to the corrected expressions, Eqs. (D3)–(D6).

Let us consider the dependences of T_c, ρ and γ with Sn content β. Experiments[3] show that T_c variation with β is essentially linear up to ~24 at% ; while between 24 and 25 at% Sn content, T_c versus β has a saturation, Fig. 1. The A15 type lattice undergoes a spontaneous cubic-tetragonal transformation in this range. The lattice softening, as one of the consequences, implies a decreasing in the lattice stiffness ($\hbar\omega_D = k_B\theta_D$) such that it reduces T_c according to McMillan T_c equation[22] [Eq. (6)]. The normal-state resistivity ρ, as measured just above T_c, decreases moderately with increase of β within 18~24 at%. Approaching $\beta = 25$ at%, $\rho(\beta)$ exhibits an obviously stronger decrease. Below 24 at%, the coefficient of electronic heat capacity, γ, changes linearly with β by ~1.5 mJ·K^{-2}·mol^{-1} per at% Sn. Following the treatment to the experimental data in ref. 3, we use global fits to the experimental T_c, γ and ρ versus β in the entire A15 range (Fig. 1 and Table 1),
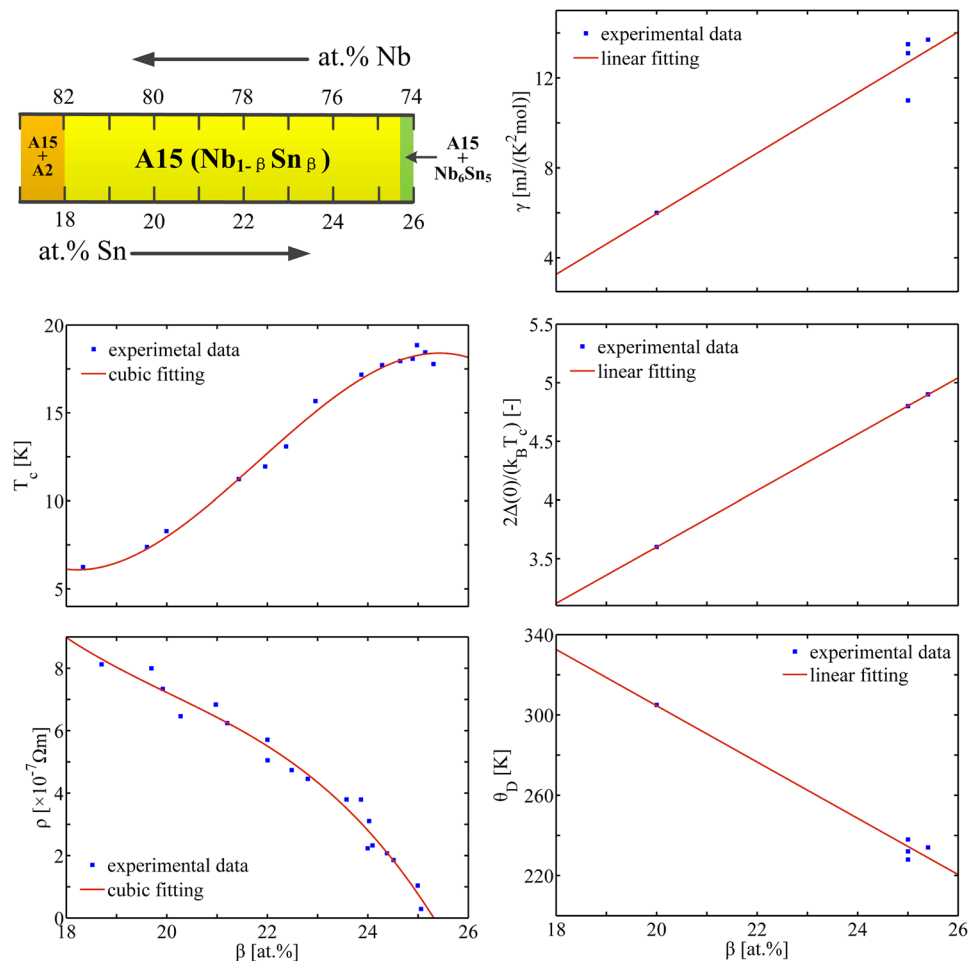
Figure 1. Variations of material parameters T_c, ρ, γ, θ_D and $2\Delta(0)/(k_B T_c)$ with Sn content β in the A15 range of binary $Nb_{1-\beta}Sn_\beta$. The experimental data are extracted from ref. 3. The solid lines represent the global fits to the experimental data in the A15 range.

χ	Linear fitting	$(\chi = a_1\beta + b_1)$		
	a_1	b_1		
γ	1.3473	−20.983		
θ_D	−14.018	584.94		
$2\Delta(0)/(k_B T_c)$	0.24043	−1.2087		
χ	Cubic fitting	$(\chi = a_2\beta^3 + b_2\beta^2 + c_2\beta + d_2)$		
	a_2	b_2	c_2	d_2
T_c	−0.065923	4.3157	−91.612	641.31
ρ	−0.021449	1.2923	−26.735	196.6

Table 1. Material parameters variation with Sn content β [at.%].

$$T_c,\ \gamma\ \text{or}\ \rho = \begin{cases} a_1\beta + b_1, & \text{linear fit,} \\ a_2\beta^3 + b_2\beta^2 + c_2\beta + d_2, & \text{cubic fit.} \end{cases} \tag{1}$$

We are now ready to calculate the dependence of the superconducting characteristic lengths $\delta_L(0)$, ξ_0 and l with the Sn concentration β, by substituting Eq. (1) into Eqs. (D4), (D5) and (D6). The London penetration depth $\delta_L(0)$ increases with Sn content, while the coherence length ξ_0 is reduced, Fig. 2. $\delta_L(0)$ and ξ_0 are roughly with the same order of magnitude over the A15 range. By comparing the coherence length ξ_0 and the electronic mean free path l, one may distinguish the clean limit, the dirty limit and the intermediate state at any A15 composition. At lower Sn content, ξ_0 maintains rather high value compared to l; but this difference is mitigated as ξ_0 continues to decrease and l increase, for rising β until the phase transformation boundary. In the tetragonal phase range, ξ_0
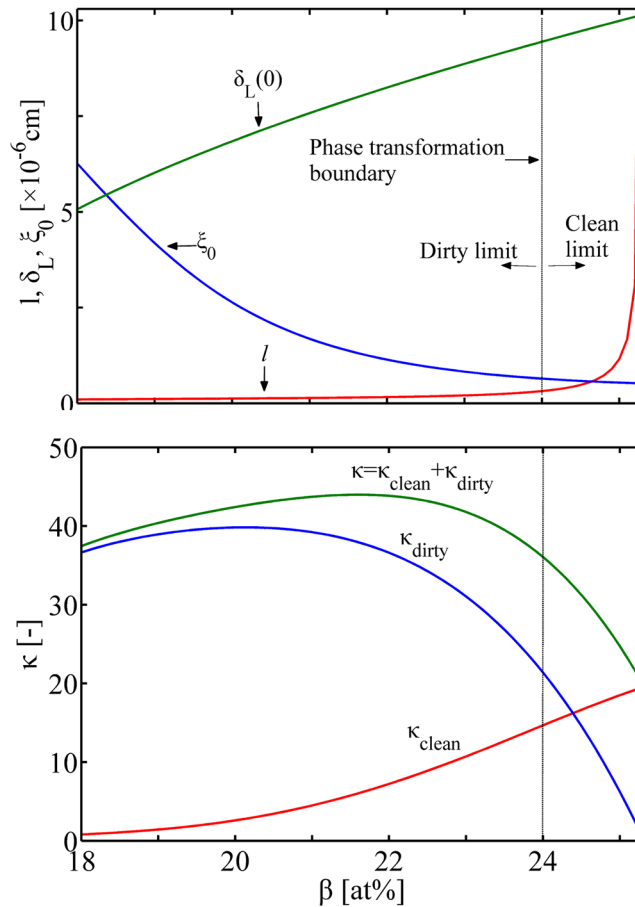
Figure 2. Composition dependence of the London penetration depth $\delta_L(0)$, coherence length ξ_0 and electronic mean free path l (Top), and the GL parameter κ (Bottom).

is approximately equal to or even lower than l. This implies that, as Sn content gradually approaches the stoichiometry, $Nb_{1-\beta}Sn_\beta$ undergoes a transition from the "dirty" limit ($\xi_0 \gg l$) to the "clean" limit ($\xi_0 \ll l$), and the phase transformation boundary may be taken as the boundary of this transition. In Fig. 2, we also present the variation of GL parameter κ with tin content, calculated by Eqs. (C19) and (D3). κ in the two limiting cases, κ_{clean} and κ_{dirty}, have the opposite change with Sn content; their change nearly counteract one another in the cubic phase range. While in the tetragonal phase range, κ_{dirty} exhibits a more severe decrease compared to the increase in κ_{clean}. Thus, $\kappa = \kappa_{clean} + \kappa_{dirty}$ varies little in the cubic phase range, but decreases largely in the tetragonal phase.

The magnetic properties of type II superconductors give $H_{c2} = \sqrt{2}\kappa H_c$ at the vicinity of T_c, where H_c is the thermodynamic critical field[23]. Combining this with the expressions κ and H_c, Eqs. (C19), (C20) and (D3), renders the upper critical field H_{c2} in the clean limit and the dirty limit, Eqs. (C14) and (D7) (see Supplementary Information C and D for detail). Thus, H_{c2} at the intermediate ξ_0/l can be obtained by summing $H_{c2,clean}$ and $H_{c2,dirty}$,

$$H_{c2} = C_1 T_c^2 (1 - T/T_c)\gamma_{mJ}^2 + C_2 T_c (1 - T/T_c)\gamma_{mJ}\rho_{\Omega m}. \tag{2}$$

Here, $C_1 = 1.979 \times 10^8 \pi^{1/3} c e^{-1} k_B^{-2} \hbar (n^{2/3} S/S_F)^{-2}$ and $C_2 = 1.356 \times 10^{-6} \pi^{-1} c e k_B^{-1}$ in which the physical constants are listed in Table A1. We have omitted multiplier $R(\lambda_{tr})$, which is defined in the Gor'kov function[19] to consider the effect of the ξ/l variations (ranging from $\xi/l \ll 1$ to $\xi/l \gg 1$), in the sum of $H_{c2,clean}$ and $H_{c2,dirty}$ [Eq. (2)]. This is reasonable since $R(\lambda_{tr})$ changes little within the entire ξ/l range[24]. The involved three material parameters T_c, γ_{mJ} and $\rho_{\Omega m}$ as well as their variations with the composition concentration in A15 $Nb_{1-\beta}Sn_\beta$ have been widely measured[3], Eq. (1) and Fig. 1. Thus, substituting Eq. (1) into Eq. (2), one finds the dependence of the upper critical field H_{c2} with Sn content. Note that the above formulas are valid at the vicinity of the superconducting transition temperature T_c.

Corrections to upper critical field for electron-phonon interaction. A15 type Nb-Sn is a strong-coupling superconductor such that the corrections for electron-phonon (EP) interaction are required. We obtain the upper critical field, Eq. (2), based on the breaking and scattering of Cooper pairs in a weak-coupled interaction. Equation (2) is corrected for EP interaction in two ways: renormalizing the material parameters, and introducing correction parameters to superconductivity itself[19, 22, 25].
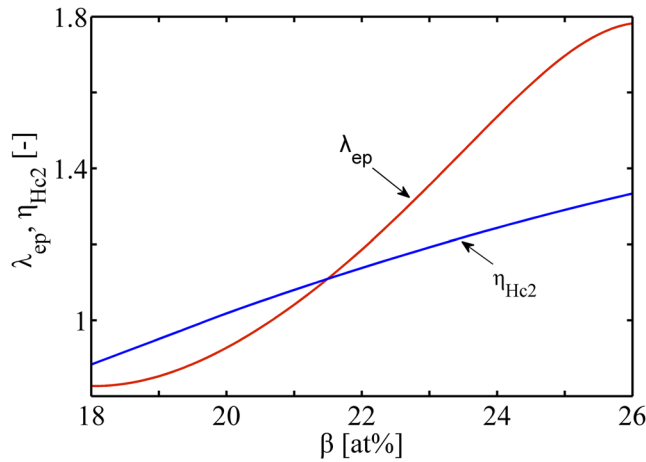
Figure 3. EP correction parameters, the Debye temperature θ_D and energy gap $\Delta(0)$, versus tin content.

We determine which material parameter should be renormalized in terms of Grimvall's principle[25]. Both the density of states and the wave function are renormalized by EP interaction, and the electron mass in the absence of EP interactions is replaced by a renormalized electron mass $m = m^b(1 + \lambda_{ep})$, where b refers to band values. The electronic density of states $\upsilon(\mu)$ at Fermi level is renormalized by an enhancement factor $1 + \lambda_{ep}$ where λ_{ep} is the EP interaction parameter, and thus the coefficient of the electronic heat capacity γ_{mJ} is enhanced by $(1 + \lambda_{ep})\gamma_{mJ}$. However, γ_{mJ} is not changed for EP renormalization in Nb_3Sn, since there are no EP renormalization effects in the change of the Fermi surface dimensions on alloy and the change in $\upsilon(\mu)$ always depends on the Fermi level and follows almost rigidly any shift in Fermi energy. The electrical resistivity $\rho_{\Omega m}$ [Eq. (A1)] is not renormalized, since the renormalization of the electron mass m exactly cancels against the renormalization of the scattering matrix element as it enters the averaged time τ between collisions. We find that, these are implicitly followed by Devantay et al.[26], who do not take renormalizations on γ_{mJ} and $\rho_{\Omega m}$. Thus, we take the only EP correction in Nb_3Sn by multiplying a factor $\eta_{H_{c2}}(T)$ for H_{c2},

$$H_{c2} = \eta_{H_{c2}}(T_c)[C_1 T_c^2(1 - T/T_c)\gamma_{mJ}^2 + C_2 T_c(1 - T/T_c)\gamma_{mJ}\rho_{\Omega m}].$$

(3)

Here, $\eta_{H_{c2}}(T_c)$ is the ratio of the strong-coupled magnetic pair-breaking parameter to the weak-coupled BCS value, and can be evaluated by the detailed EP spectrum[24].

If T_c and the energy gap $\Delta(0)$ at 0 K are determined experimentally, we have the strong-coupling correction $\eta_{\Delta(0)}$ to $\Delta(0)$, $\eta_{\Delta(0)} = (2\Delta(0)/k_B T_c)_{meas}/(2\Delta(0)/k_B T_c)_{BCS} = (2\pi/\eta)^{-1}(2\Delta(0)/k_B T_c)_{meas} \approx 0.283(2\Delta(0)/k_B T_c)_{meas}$ in which the BCS equation $\Delta(0) = (\pi/\eta)k_B T_c$ with $\eta = 1.78$ has been used for the second equal sign. The characteristic (equivalent Einstein) frequency ω_0 [erg] is then determined using[19] (Supplementary Information E)

$$\eta_{\Delta(0)} = 1 + 5.3(\omega_0 k_B^{-1} T_c^{-1})^{-2} \ln(\omega_0 k_B^{-1} T_c^{-1}).$$

(4)

The EP correction to H_{c2}, $\eta_{H_{c2}}(T_c)$, can thus be obtained,

$$\eta_{H_{c2}}(T_c) = 1 + \pi^2(\omega_0 k_B^{-1} T_c^{-1})^{-2}[0.6 \ln(\omega_0 k_B^{-1} T_c^{-1}) - 0.26].$$

(5)

The another correction parameter (not involved in EP correction for Nb_3Sn), i.e. the EP interaction parameter λ_{ep}, is determined by the McMillan strong-coupled T_c equation[22]

$$T_c = \frac{\theta_D}{1.45}\exp\left(-\frac{1.04(1 + \lambda_{ep})}{\lambda_{ep} - \mu^*(1 + 0.62\lambda_{ep})}\right),$$

(6)

where θ_D is the Debye temperature and μ^* is the pseudo potential parameter for electron Coulomb repulsion (for Nb_3Sn $\mu^* \approx 0.2$). Note that to obtain a more accurate λ_{ep} for Nb_3Sn one should use the Allen-Dynes T_c formula, which extends the application range $0 < \lambda_{ep} < 1.5$ of Eq. (6) to a large λ_{ep} value. Experiments give $\lambda_{ep} \approx 1.8$ for Nb_3Sn. However, the available experimental data is θ_D and not the characteristic phonon frequency required in the Allen-Dynes T_c formula. Thus we still apply Eq. (6) at the cost of some accuracy.

The corrections for EP interaction require the information of the Debye temperature θ_D and the energy gap $\Delta(0)$ at 0 K, Eq. (3). Unfortunately, the available data are reported at very limited Sn content. We use linear fits to θ_D and $(2\Delta(0)/k_B T_c)$ according to the identification[3] of the gradual changes from strong coupling to weak coupling with decreasing β, Fig. 1.

Figure 3 presents the calculated EP correction parameters in terms of Eqs. (1), (5) and (6). The result of the strong-coupling correction $\eta_{H_{c2}}$ to H_{c2} approximately equals to the calculated value[19] of 1.17 at $T_c = 17.8$ K. The

calculated EP interaction parameter λ_{ep} at the stoichiometry 25 at% Sn is slightly lower than the generally accepted value of 1.8[27]. However, at larger derivation from the stoichiometry, the calculated λ_{ep} differs relatively larger from the value of 1.8.

Upper critical field at temperature 0 K. In the following we will concern the behavior of H_{c2} at temperatures far from T_c, where the GLAG theory does not apply. This will generalize the above results near T_c [e.g. Eq. (3)] to a wide temperature range and up to 0 K. The temperature dependence of H_{c2} in the scaling law for Nb_3Sn is determined by an approximate form of the Maki-de Gennes (MDG) relation[28],

$$H_{c2}(T) = H_{c2}(0)[1 - (T/T_c)^\lambda]. \tag{7}$$

Recent measurements suggest $\lambda \approx 1.52$; this value has a universe applicability to a wide range of off-stoichiometric samples and different methods of determining H_{c2}[10]. This value of λ is also the power determined from the MDG theory and Eliashberg theory[28, 29]. Godeke et al. demonstrate that the MDG description (7) is universal for $H_{c2}(T)$ relation of $Nb_{1-\beta}Sn_\beta$ independent of the compositional variation[2, 10]. Recent experiment shows that this relation is applicable for Nb_3Sn with or without undergoing the cubic-to-tetragonal transition[11]. We are then allowed to extrapolate H_{c2} at vicinity of T_c to $H_{c2}(0)$ at temperature 0 K for any Sn content. If $H_{c2}(T_0)$ with $T_0 \to T_c$ has been obtained using Eq. (3), then one can deduce $H_{c2}(0)$ as

$$H_{c2}(0) = H_{c2}(T_0)/[1 - (T_0/T_c)^\lambda]. \tag{8}$$

We assume that EP interaction correction to H_{c2} far from T_c is the same as that for H_{c2} near T_c.

WHH (Werthamer-Helfand-Hohenberg) equation, derived from Gor'kov superconductivity theory (Green function method) and taking into account electron spin and spin-orbital scattering[30], is capable of giving rather satisfactory descriptions for H_{c2} behavior of a wide range of commercial and experimental Nb_3Sn wires. This equation can be written as a simple form

$$H_{c2}(0) = 0.69H'_{c2}T_c, \tag{9}$$

where $H'_{c2} = -(dH_{c2}dT)_{T_c}$[13]. Substituting the derivative of Eq. (3) into Eq. (9) and then comparing to Eq. (3), one finds $H_{c2}(0) = 0.69H_{c2}(T_0)/(1 - T_0/T_c)$. It is further shown that the only difference between WHH equation and MDG relation is the power of (T_0/T_c); Since $T_0/T_c \to 1$ this difference has very limited impact on the $H_{c2}(0)$ values. This is consistent with the viewpoint[30, 31] that MDG relation is a good approximation to Werthamer theory.

We now calculate the upper critical field B_{c2} near T_c using Eqs. (1), (2) and (3), Fig. 4. The temperature T_0 near T_c is designated as $T_0 = 0.9T_c$. One finds the dependence of $B_{c2}(T_0)$ on Sn content β with/without the EP correction. The results of $B_{c2}(T_0)$ are then substituted into the MDG relation, Eq. (8), to obtain B_{c2} at 0 K, $B_{c2}(0)$. Since the WHH relation is equivalent to the MDG relation, we do not implement it redundantly. The calculation results are impressive (Fig. 4): $B_{c2}(0)$ obtained by $B_{c2}(T_0)$ with EP correction and then extrapolated by MDG relation (EP + MDG) is in good agreement with the experiments. This validates the above GLAG descriptions, and also the MDG description for the temperature dependence of the upper critical field at any composition over the A15 phase field.

We find that, the cubic-tetragonal phase boundary at ~24 at% Sn separates the increasing B_{c2} versus β from the decreasing B_{c2} versus β. As shown both in the experimental $B_{c2}(0)$ versus tin content and the EP + MDG curve, the maximum ~29 T of $B_{c2}(0)$ appears at ~24 at% Sn, and at both sides of the peak, $B_{c2}(0)$ decreases as tin content deviates more from 24 at% Sn. In the tetragonal phase, $B_{c2}(0)$ has a more serious reduction; however, at the vicinity of 24 at% Sn, $B_{c2}(0)$ have nearly the same values at both sides of 24 at% Sn, namely in the cubic phase range and the tetragonal phase range. This is consistent with the experiment by Zhou et al.[11], their tetragonal phase [$B_{c2}(0.3 K) = 29.1$ T at $\beta = 24.6 \pm 0.2$ at%] and cubic phase [$B_{c2}(0.3 K) = 29.0$ T at $\beta = 23.7 \pm 0.4$ at%] samples exhibiting almost identical $B_{c2}(0) \approx 29 \pm 0.2$ T. We infer that, this coincidence occurs in a limited range, where the tin content deviates small from the phase transformation boundary; for a large deviation there is a stronger depression of $B_{c2}(0)$ in the tetragonal phase. This phenomenon is caused by the underlying relationship between the superconductivity of Nb_3Sn and the related material parameters; physical properties of the latter is continually changed by the spontaneous cubic-tetragonal transformation.

We now consider the upper critical field $B_{c2}(0)$ decomposing into the component in the clean limit case [Eq. (D7)] and that in the dirty limit case [Eq. (C14)], $B_{c2}(0) = B_{c2,clean} + B_{c2,dirty}$. One finds that $B_{c2,clean}$ increases as β raised, but for contrast the dirty one increases up to 24 at% and then deceases drastically, Fig. 5. As we already know, $Nb_{1-\beta}Sn_\beta$ undergoes a transition from the "dirty" limit to "clean" limit as β increased. By comparing Figs 4 and 5, we find that, within 18 at%~24 at%, the component $B_{c2,dirty}$ dominates in $B_{c2}(0)$ and determines the trend of $B_{c2}(0)$ curve. Once crossing over the phase transformation boundary, $B_{c2,clean}$ takes over $B_{c2}(0)$ variation with β.

Limit for upper critical field: Pauli paramagnetic limit. Preferential Pauli-paramagnetic lowering of normal-state free energy should place a limit on the orbital-pair-breaking H_{c2} of filamentary high-field superconductor[32],

$$H_{c2}(0) \leq H_p(0) \equiv 1.84 \times 10^4 T_c[\text{Oe}]. \tag{10}$$

This equation is a rough estimation for the limit field $H_p(0)$, since the assumption that the zero temperature difference between superconducting and normal-state magnetizations be at least equal to the Pauli conduction-electron-spin magnetization, is somewhat contrary to experimental results[33]. The correction to $H_p(0)$ for EP interaction is given by
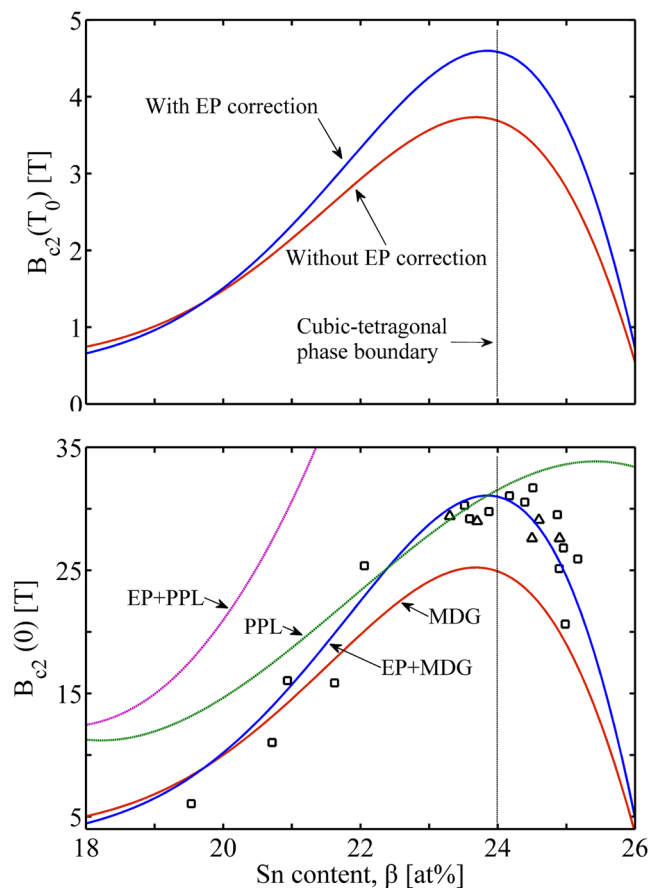
Figure 4. Upper critical field B_{c2} variation as a function of tin content β at: the vicinity of T_c (Top) and 0K temperature (Bottom). MDG: extrapolation of $H_{c2}(T_c)$ with MDG relation, Eqs. (1), (2) and (8); EP + MDG: extrapolation of EP corrected $H_{c2}(T_c)$ with MDG, Eqs. (1), (2), (3) and (8); PPL: Pauli paramagnetic limit, Eqs. (1) and (10); EP + PPL: EP corrected Pauli paramagnetic limit, Eqs. (1) and (11); □: Experiment dataset-1[3]; △: Experiment dataset-2[11].
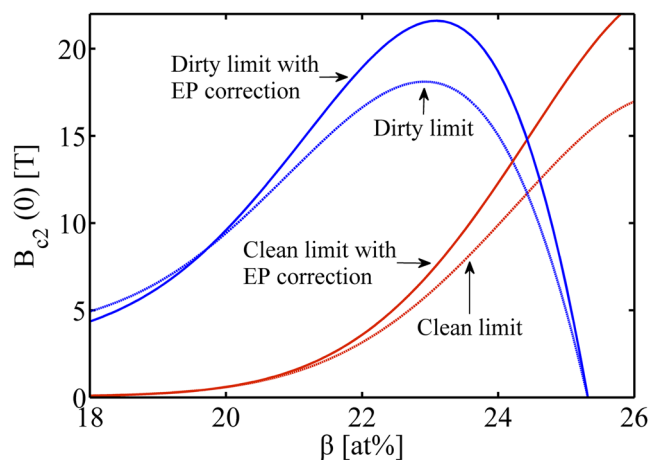
Figure 5. Upper critical field $B_{c2}(0)$ in the clean and dirty limit case.

$$H_p(0) = 1.84 \times 10^4 \eta_{H_c}(0)(1 + \lambda_{ep})^{1/2} T_c [\text{Oe}], \tag{11}$$

where $\eta_{H_c}(T_c) = 1 + \pi^2(\omega_0 k_B^{-1} T_c^{-1})^{-2}[1.1\ln(\omega_0 k_B^{-1} T_c^{-1}) + 0.14]$ assuming $\eta_{H_c}(T)$ is independent with temperature[19].
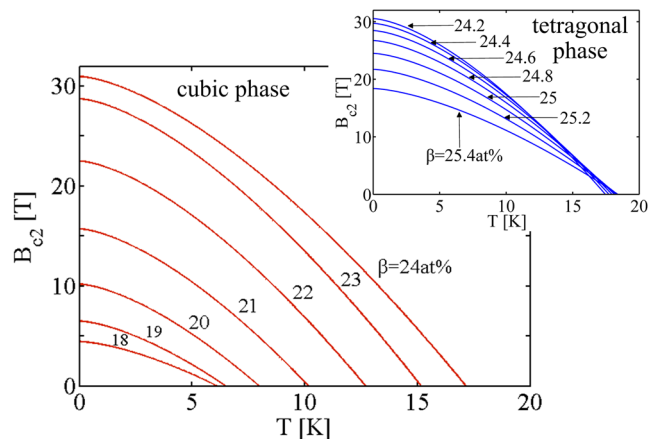
Figure 6. Temperature dependence $B_{c2}(T)$ at varying Sn content in the range of the cubic phase at increment of 1 at% from 18 at% to 24 at% Sn. The insert figure represents the situation in the tetragonal phase for 0.2 at% increment between 24.2 at% and 25.4 at% Sn.

Samples	β[at%] $\rho(T_c)$ [$\mu\Omega\cdot$cm]	$\rho(T_c)$[$\mu\Omega\cdot$cm]	γ[mJ/molK²]	T_c[K]	$B_{c2}(0)$[T]
Thin films by Orlando *et al.*[19]	−/23.59[(a)] −/24.94	35/35 9/9.1	−/10.8 −/12.6	16.0/16.4 17.4/18.2	29.5/30.8 26.3/25.2
Bulk by Godeke *et al.*[2]	−/24.33 −/24.33	22(50%)/22.0 22(90%)/22.0	−/11.8 −/11.8	16.5/17.6 16.6/17.6	27.4/30.1 28.3/30.1
Polycrystal by Guritanu *et al.*[18]	−/24.46	−/19.4	13.7/11.8	17.8/17.8	25.0/29.4

Table 2. Calculated *H-T* phase boundary and comparison to experiments. [(a)]Before the oblique line is the experimental value and after that presents the calculated value.

In Fig. 4, PPL (Pauli paramagnetic limit), Eqs. (1) and (10), slightly lowers the EP + MDG curve after ~23 at% Sn, and it thus provides a good boundary with the experimental data before the phase transformation. This justifies that, PPL is independent with the EP interaction in Nb_3Sn. In Fig. 4, EP corrected PPL [Eqs. (1) and (11)] is much higher than the experimental curve and has no restriction to $B_{c2}(0)$. This is consistent with the view by Orlando *et al.*[19], who demonstrate that EP corrected PPL has nothing to do with Nb_3Sn superconductivity, since the strong EP interaction in Nb_3Sn increases largely the Pauli limiting field above its BCS value and the spin-orbit scattering is less involved. This explains why we only take the impurity scattering into account while exclude the spin-orbit scattering.

Results and Discussion

Temperature dependence of upper critical field. Now, we focus on the temperature dependence of B_{c2} at any A15 composition concentration, Eqs. (1), (3), (7) and (8). In Fig. 6, the temperature dependence $B_{c2}(T)$ increases at any temperature as raising the Sn content β within the cubic phase range. The tetragonal phase exhibits a reverse behavior, B_{c2} at 0 K and at most of other temperatures increasing with reduced Sn content. Orlando *et al.* show that in thin films $B_{c2}(0)$ is increased with ρ rising, however T_c is suppressed[2, 19]. For $\rho(T_c) = 35\,\mu\Omega\cdot$cm, there exists $B_{c2}(0) = 29.5$ T and $T_c = 16.0$ K; while $\rho(T_c) = 9\,\mu\Omega\cdot$cm leads to $B_{c2}(0) = 26.3$ T and $T_c = 17.4$ K[19]. This corresponds to the calculated composition dependence in the tetragonal phase range, Figs 1 and 6. The measured bulk needle by Godeke *et al.* exhibits a similar behavior: $\rho(T_c) = 22\,\mu\Omega\cdot$cm at a 50% normal-state resistance criterion corresponds to $B_{c2}(0) = 27.4$ T and $T_c = 16.5$ K, and at a 90% criterion $B_{c2}(0) = 28.3$ T and $T_c = 16.6$ K[2]. A summary of the calculations and the comparisons to experiments is given in Table 2. Through the theoretical expressions, we also figure out the material parameter that is undetermined by experiments, Table 2.

We also calculate $B_{c2}(T)$ for two rather highly homogenous Nb_3Sn samples, Fig. 7. Their material parameters, reproduced from[11], are listed in the insert of the figure. Note that in the absence of the raw experimental value of γ, we infer it from Eq. (1). Calculations show that, the dirtier sample (25 Sn-1800) with the larger resistivity (31.3 $\mu\Omega\cdot$cm) always exhibits a higher B_{c2} at any temperature while T_c is suppressed. This follows the above observation by Orlando *et al.*[19] and Godeke *et al.*[2]. The little discrepancy from the experiment may be attributed to the absence of the raw data of γ and the greater uncertainty in experimentally determining the composition concentration (fluctuation of ±0.7 at% Sn for the dirtier sample compared to ±0.2 at% for the cleaner one).

Flux pinning force and Kramer plot. We now extend the method for the upper critical field B_{c2} to account for the pinning behavior at different composition concentrations. Using the flux pinning model proposed by Kramer[34], the pinning force per volume for Nb_3Sn conductors, $F_p(B)$, is given by[10]
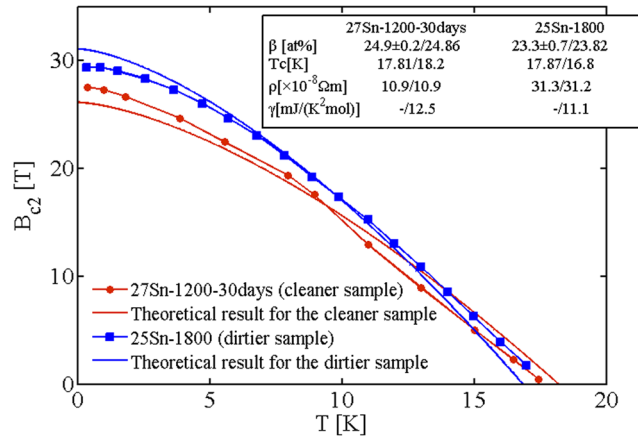
Figure 7. Temperature dependence $B_{c2}(T)$ for two homogenous off-stoichiometric Nb$_3$Sn samples, and comparison to experiments[11].

$$F_p(B) = J_c B = 12.8 \kappa^{-2} B_{c2}^{2.5} (B/B_{c2})^{0.5} (1 - B/B_{c2})^2 \ [\text{GN} \cdot \text{m}^{-3}], \tag{12}$$

where J_c is the critical current density. $F_p(B)$ is associated with Sn concentration through the composition dependences $B_{c2}(T, \beta)$ and $\kappa(\beta)$, which are formulated by Eqs. (1), (3), (7), (8), (C19) and (D3). The Kramer function $f_K(B) = J_c^{0.5} B^{0.25}$ is linear with the magnetic induction B and can identify B_{c2} at which $f_K(B) = 0$[10],

$$f_K(B) = J_c^{0.5} B^{0.25} = 1.1 \times 10^5 \kappa^{-1} (B_{c2} - B) [\text{A}^{0.5} \text{m}^{-1} \text{T}^{0.25}]. \tag{13}$$

From Fig. 8 we observe a profound influence of the composition concentration on the field dependent pinning force $F_p(B)$. Within the cubic phase range, the increase of Sn content raises the $F_p(B)$ remarkably and shifts the peak in each $F_p(B)$ curve to the high field region. This is associated with the composition dependent superconducting properties. To be specific, the magnitude of B_{c2} determines the position of the peak in $F_p(B)$, while the height of $F_p(B)$ is related to both B_{c2} and κ, Eq. (12). B_{c2} in the cubic phase range increases as β rising (Fig. 4) while κ varies little (Fig. 2), thus resulting in the shift of the peak and the increase in the height of $F_p(B)$. This case differs from that for the tetragonal phase range, where rising β leads to a drastic decrease in both B_{c2} and κ. As in Fig. 8, the peak shifts to the lower field and the height is nearly the same in all curves (due to $F_p(B) \propto \kappa^{-2} B_{c2}^{2.5}$). The experimental data of a Nb$_3$Sn conductor locate roughly between the calculated $F_p(B)$ curves for different Sn contents. This implies that, to describe a real Nb$_3$Sn conductor one may consider the composition gradient in the conductor which results in a weighted average of local homogenous composition properties. For Kramer plot, we find its variation consistent with $F_p(B)$ for the similar reasons (Fig. 8).

Composition gradient effect on practical Nb$_3$Sn wires. In the following we will apply our descriptions for the superconducting properties variation with tin content in the concentric shells model proposed by Cooley et al.[7], to arrive at the real composition dependent behavior in practical Nb$_3$Sn conductors. In the Nb$_3$Sn filament of PIT wires, the A15 layer exists between a central Sn-rich core and a coaxial Nb tube, Fig. 9. This structure is convenient for using a series of concentric shells with varying Sn concentration to simulate the composition inhomogeneity in the wire. The Sn content β varies with the position in the A15 layer[7],

$$\beta = 18 + 3.5[1 - r^N + (1 - r)^{1/N}] \ [\text{at\%}], \tag{14}$$

where N indicates the severity and steepness of the overall gradient and r is the normalized radius of the filament cross section. The radius r is set to be 0 at the A15/Sn-core interface and reaches its maximum 1 at the Nb/A15 interface. The actual position in this area is counted as $R = 10 + 5r$ [μm], indicating that the inner radius of the A15 layer is $R_{\min} = 10$ μm and the outer radius is $R_{\max} = 15$ μm.

For PIT wires, the prefactor of the flux pinning force differs from the Kramer model [Eq. (13)], $F_p(B) = J_c B = 0.35 B_{c2}^2 (B/B_{c2})^{0.5} (1 - B/B_{c2})^2 [\text{GN} \cdot \text{m}^{-3}]$ and $f_K(B) = 1.871 \times 10^4 B_{c2}^{-0.25} (B_{c2} - B) [\text{A}^{0.5} \text{m}^{-1} \text{T}^{0.25}]$. We can then link $B_{c2}(T, \beta)$ and J_c to the radius r, and the local magnetic moment is calculated as $m_o = \pi R^2 t L J_c$ [Am^2], where t is the thickness of each of the 100 shells, i.e. $t = (R_{\max} - R_{\min})/100$ and L is the sample length.

Figure 9 presents the Sn content variation with the radius r at different gradients N. It is found that, larger steepness of the overall gradient N has a more drastic decrease near the outer radius (closer to the real situation). The distribution of the magnetic moment m_o along the radius r at different applied magnetic fields is also presented in Fig. 9. At any magnetic field B, the regions near the Nb/Nb$_3$Sn ($r = 1$) and/or Nb$_3$Sn/Sn-core ($r = 0$) interfaces appear no magnetic moment and thus loss of superconductivity. The larger region of the loss occurs for the higher magnetic field, with a suppression in the magnitude of magnetic moment. In fact, the magnetic moment is related to the local critical current density and thus the pinning force $F_p(B)$. One can find the Sn content dependence of $F_p(B)$ from Fig. 8; in the cubic phase range, $F_p(B)$ is raised with the Sn content increasing at
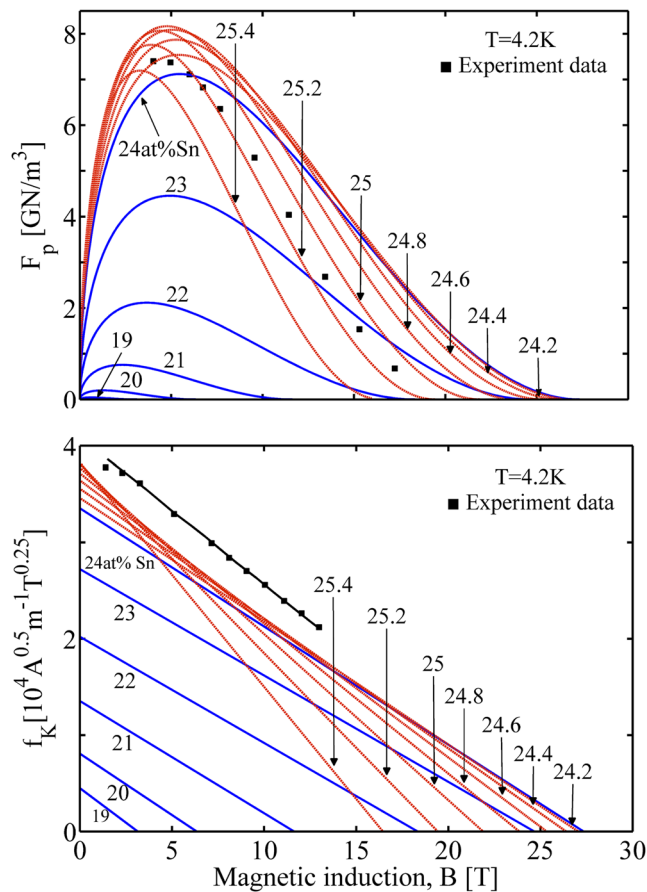
Figure 8. Effect of composition concentration on the magnetic field dependence of the flux pinning force (Top) and Kramer plot (Bottom). The experiment data are extracted from refs 10 and 28.
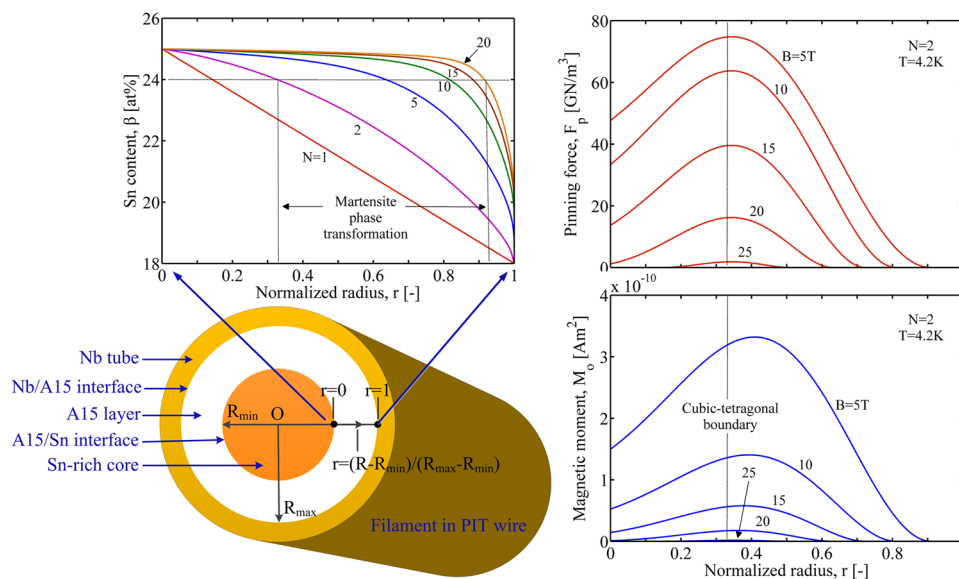
Figure 9. Distribution of the Sn content β (Top left), pinning force F_p (Top right) and magnetic moment m_o (Bottom right) on the cross section of PIT wire filament (Bottom left), at temperature $T = 4.2$ K. N indicates the severity of the overall gradient.
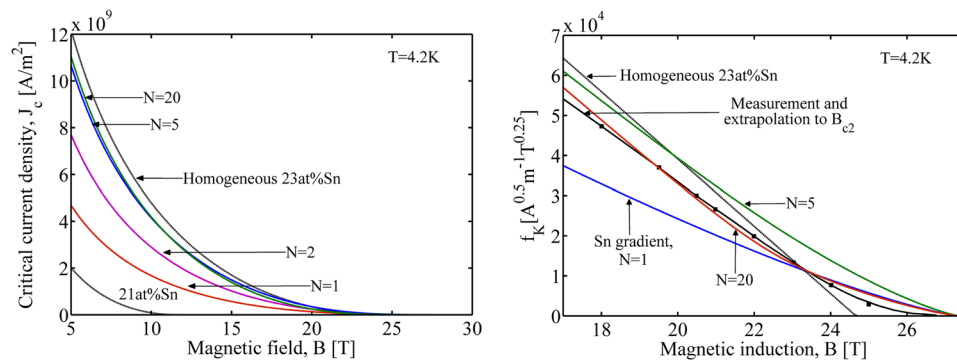
Figure 10. Effect of the composition gradient on the critical current density (Left) and Kramer function $J_c^{0.5}B^{0.25}$ (Right) of PIT wires. The measurements on SMI ternary PIT wire are duplicated from ref. 2. The Kramer plot with a composition gradient $N = 20$ has a positive curvature approaching the experiment.

any field, and F_p for lower Sn content more probably turns to disappear at higher fields. These are the underlying reasons for the vanishing of the magnetic moment. The tetragonal phase has a similar corresponding relationship. So, the loss of superconductivity near the boundary of A15 layer is mainly associated with the change of the flux-pinning behavior due to the A15 composition variation.

Summing the contributions m_o from each shell results in the total magnetic moment m_{ot}, which can be measured by magnetometry. The critical current density J_c of the wire is then expressed as $J_c = 3m_{ot}/[\pi L(R_{max}^3 - R_{min}^3)]$ $[A/m^2]$ in a longitudinal field[7]. In Fig. 10, we present the variation of J_c as a function of the magnetic field B for different Sn gradients N. The homogenous sample results are presented to emphasize the effect of the tin gradient. The results of $J_c(B)$ allow one to depict the Kramer plot $f_k(B)$. The Kramer plot[2] for the measurements on a SMI ternary PIT wire exhibits an anomalous curvature "tail" at the vicinity of B_{c2}, Fig. 10. Two calculated homogenous samples with 21 at% and 23 at% appear no curvature, however, the inhomogeneous samples have a curved $f_k(B)$ when approaching B_{c2}. An acceptable agreement with the experiment is found for the conductor with gradient severity $N = 20$. At this point, we reproduce the positive curvature in the Kramer plot of the PIT wire, emphasizing the importance of the composition inhomogeneity in the superconducting properties of practical Nb$_3$Sn conductors. The composition dependent pinning force and Kramer function explain the disagreement between the results of the scaling laws and the experiments for practical inhomogeneous conductors.

Conclusions

Although Nb$_3$Sn has been extensively used in fusion engineering area like ITER, the dependence of the superconducting properties with inhomogeneous composition is established incompletely in theory. Based on the GLAG theory frame, we derive a series of expressions for the superconductivity parameters [Eq. (1)] and the upper critical field as a function of the three material parameters [Eq. (2)]. These relations have a complete self-consistent theory basis describing the variation of superconductivity of Nb$_3$Sn with Sn content. The corrections for EP interaction are included [Eq. (3)]. The theoretical estimation of $H_{c2}(0)$ variation with Sn content [Eqs. (3) and (8)], provided with the fits to the material parameters, shows an acceptable agreement with the experiments.

A15-type Nb-Sn undergoes a transition from "dirty" limit ($\xi_0 \gg l$) to "clean" limit ($\xi_0 \ll l$) as Sn content gradually approaches the stoichiometry [Eqs. (C19), (D4), (D5), (D6) and (D3)]. The change in superconductivity at the vicinity of the critical temperature and in the related material parameters determines the composition dependence of the upper critical field. The MDG description [Eq. (7)] is universal for describing H-T phase boundary over the A15 phase field.

In the cubic phase range, $B_{c2}(T)$ increases with raising Sn content [Eqs. (1), (3), (7) and (8)]. There appears an inverse $B_{c2}(T)$ behavior in the tetragonal phase range. A significant influence of the composition concentration on $F_p(B)$ [Eqs. (12) and (13)] curves is observed. Within the cubic phase range, the increase of Sn content raises the $F_p(B)$ remarkably and shifts the peak in each $F_p(B)$ curve to the right side. The peak shifts to the lower field and the shape is nearly the same in the tetragonal range. This can be explained by the composition dependencies $B_{c2}(T,\beta)$ and $\kappa(\beta)$.

The effect of composition gradient on the superconducting properties of PIT wires is considered by applying the obtained formulas in Cooley's concentric shells model [Eq. (14)]. The loss of superconductivity near the boundary of A15 layer is mainly associated with the change of the flux-pinning behavior due to the A15 composition variation. The inhomogeneous conductor with gradient severity $N = 20$ predicts well the curved "tail" approaching B_{c2} in the Kramer plot. This implies that the composition inhomogeneity is an important factor in the unusual phenomenon of the practical Nb$_3$Sn conductors.

However, we cannot yet include the effect of the alloying addition (Ti and/or Ta) and the matrix material (bronze and/or copper) in a ternary Nb$_3$Sn wire. The composition gradient is an important factor in the unusual phenomenon of practical Nb$_3$Sn conductors but not the unique determinant. The most possible role of the alloying addition taken in Nb$_3$Sn is the scattering impurity (Supplementary Information A), which changes the electrical resistivity deeply. We will include this effect in the future work to increase the practical value of the present theory.

References

1. Minervini, J. V. Superconductivity: Squeezing out the current. *Nature materials* **13**, 326–327, doi:10.1038/nmat3931 (2014).
2. Godeke, A. *et al*. The upper critical field of filamentary Nb₃Sn conductors. *Journal of Applied Physics* **97**, 093909, doi:10.1063/1.1890447 (2005).
3. Flükiger, R., Uglietti, D., Senatore, C. & Buta, F. Microstructure, composition and critical current density of superconducting Nb₃Sn wires. *Cryogenics* **48**, 293–307, doi:10.1016/j.cryogenics.2008.05.005 (2008).
4. Godeke, A. A review of the properties of Nb₃Sn and their variation with A15 composition, morphology and strain state. *Superconductor Science and Technology* **19**, R68–R80, doi:10.1088/0953-2048/19/8/R02 (2006).
5. Tarantini, C. *et al*. Composition and connectivity variability of the A15 phase in PIT Nb₃Sn wires. *Superconductor Science and Technology* **28**, 095001, doi:10.1088/0953-2048/28/9/095001 (2015).
6. Vieland, L., Cohen, R. W. & Rehwald, W. Evidence for a first-order structural transformation in Nb₃Sn. *Physical Review Letters* **26**, 373–376, doi:10.1103/PhysRevLett.26.373 (1971).
7. Cooley, L. D., Fischer, C. M., Lee, P. J. & Larbalestier, D. C. Simulations of the effects of tin composition gradients on the superconducting properties of Nb₃Sn conductors. *Journal of Applied Physics* **96**, 2122–2130, doi:10.1063/1.1763993 (2004).
8. Xu, X., Sumption, M., Peng, X. & Collings, E. W. Refinement of Nb₃Sn grain size by the generation of ZrO₂ precipitates in Nb₃Sn wires. *Applied Physics Letters* **104**, 082602-082602-082604 (2014).
9. Marzi, G. D. *et al*. Reversible stress-induced anomalies in the strain function of Nb₃Sn wires. *Superconductor Science and Technology* **25**, 025015, doi:10.1088/0953-2048/25/2/025015 (2012).
10. Godeke, A., ten Haken, B., ten Kate, H. H. J. & Larbalestier, D. C. A general scaling relation for the critical current density in Nb₃Sn. *Superconductor Science and Technology* **19**, R100–R116, doi:10.1088/0953-2048/19/10/R02 (2006).
11. Zhou, J. *et al*. Evidence that the upper critical field of Nb₃Sn is independent of whether it is cubic or tetragonal. *Applied Physics Letters* **99**, 122507, doi:10.1063/1.3643055 (2011).
12. Senatore, C. & Flükiger, R. Formation and upper critical fields of the two distinct A15 phases in the subelements of powder-in-tube Nb₃Sn wires. *Applied Physics Letters* **102**, 012601, doi:10.1063/1.4773490 (2013).
13. Cooley, L. D., Hu, Y. F. & Moodenbaugh, A. R. Enhancement of the upper critical field of Nb₃Sn utilizing disorder introduced by ball milling the elements. *Applied Physics Letters* **88**, 142506, doi:10.1063/1.2193047 (2006).
14. Baumgartner, T. *et al*. Assessing composition gradients in multifilamentary superconductors by means of magnetometry methods. *Superconductor Science and Technology* **30**, 014011, doi:10.1088/0953-2048/30/1/014011 (2016).
15. Xu, X. & Sumption, M. D. A model for the compositions of non-stoichiometric intermediate phases formed by diffusion reactions, and its application to Nb(3)Sn superconductors. *Scientific Reports* **6**, 19096, doi:10.1038/srep19096 (2016).
16. Lee, P. J. & Larbalestier, D. C. Microstructural factors important for the development of high critical current density Nb₃Sn strand. *Cryogenics* **48**, 283–292, doi:10.1016/j.cryogenics.2008.04.005 (2008).
17. Xu, X., Sumption, M. D. & Peng, X. Internally oxidized Nb₃Sn strands with fine grain size and high critical current density. *Advanced Materials* **27**, 1346–50, doi:10.1002/adma.201404335 (2015).
18. Guritanu, V. *et al*. Specific heat of Nb₃Sn: The case for a second energy gap. *Physical Review B* **70**, 184526, doi:10.1103/PhysRevB.70.184526 (2004).
19. Orlando, T., McNiff, E., Foner, S. & Beasley, M. Critical fields, Pauli paramagnetic limiting, and material parameters of Nb₃Sn and V₃Si. *Physical Review B* **19**, 4545–4561, doi:10.1103/PhysRevB.19.4545 (1979).
20. Abrikosov, A. A. *Fundamentals of the Theory of Metals* (Elsevier, 1988).
21. Wiesmann, H. *et al*. Estimate of density-of-states changes with disorder in A-15 superconductors. *Physical Review B* **17**, 122–125, doi:10.1103/PhysRevB.17.122 (1978).
22. McMillan, W. Transition Temperature of Strong-Coupled Superconductors. *Physical Review* **167**, 331–344, doi:10.1103/PhysRev.167.331 (1968).
23. Abrikosov, A. Nobel lecture: Type-II superconductors and the vortex lattice. *Reviews of modern physics* **76**, 975–979, doi:10.1103/RevModPhys.76.975 (2004).
24. Werthamer, N. & McMillan, W. Temperature and Purity Dependence of the Superconducting Critical Field H_c2. IV. Strong-Coupling Effects. *Physical Review* **158**, 415–417, doi:10.1103/PhysRev.158.415 (1967).
25. Grimvall, G. The electron-phonon interaction in normal metals. *Physica Scripta* **14**, 63–78, doi:10.1088/0031-8949/14/1-2/013 (1976).
26. Devantay, H., Jorda, J., Decroux, M., Muller, J. & Flükiger, R. The physical and structural properties of superconducting A15-type Nb-Sn alloys. *Journal of Materials Science* **16**, 2145–2153, doi:10.1007/BF00542375 (1981).
27. Valentinis, D. F., Berthod, C., Bordini, B. & Rossi, L. A theory of the strain-dependent critical field in Nb₃Sn, based on anharmonic phonon generation. *Superconductor Science and Technology* **27**, 025008, doi:10.1088/0953-2048/27/2/025008 (2014).
28. Ekin, J. W. Unified scaling law for flux pinning in practical superconductors: I. Separability postulate, raw scaling data and parameterization at moderate strains. *Superconductor Science & Technology* **23**, 083001 (2010).
29. Oh, S. & Kim, K. A scaling law for the critical current of Nb₃Sn stands based on strong-coupling theory of superconductivity. *Journal of Applied Physics* **99**, 033909, doi:10.1063/1.2170415 (2006).
30. Werthamer, N. R., Helfand, E. & Hohenberg, P. C. Temperature and purity dependence of the superconducting critical field, H_c2. III. Electron spin and spin-orbit effects. *Physical Review* **147**, 295–302, doi:10.1103/PhysRev.147.295 (1966).
31. Taylor, D. M. J. & Hampshire, D. P. The scaling law for the strain dependence of the critical current density in Nb₃Sn superconducting wires. *Superconductor Science and Technology* **18**, S241–S252, doi:10.1088/0953-2048/18/12/005 (2005).
32. Clogston, A. M. Upper limit for the criticalfield in hard superconductors. *Physical Review Letters* **9**, 266–267, doi:10.1103/PhysRevLett.9.266 (1962).
33. Hake, R. R. Upper-critical-field limits for bulk type-II superconductors. *Applied Physics Letters* **10**, 189–192, doi:10.1063/1.1754905 (1967).
34. Kramer, E. J. Scaling laws for flux pinning in hard superconductors. *Journal of Applied Physics* **44**, 1360–1370, doi:10.1063/1.1662353 (1973).

Acknowledgements

Author Contributions

Y.L. initiated this study, developed the model, and wrote the manuscript. Y.G. supported this work, discussed the results, and reviewed the manuscript.

Additional Information

Supplementary information accompanies this paper at doi:10.1038/s41598-017-01292-4

Competing Interests: The authors declare that they have no competing interests.

Publisher's note: Springer Nature remains neutral with regard to jurisdictional claims in published maps and institutional affiliations.